Journal of Biochemistry and Molecular Biology, Vol. 40, No. 5, September 2007, pp. 649-655

JOURNAL OF Biochemistry and Molecular Biology

Biochemical Characterization of Exoribonuclease Encoded by SARS Coronavirus

Ping Chen[1], Miao Jiang[1], Tao Hu[1], Qingzhen Liu[1], Xiaojiang S. Chen[2] and Deyin Guo[1,*]

[1]State Key Laboratory of Virology and The Modern Virology Research Centre, College of Life Sciences, Wuhan University, Wuhan 430072, P.R. China

[2]Department of Molecular and Computational Biology, University of Southern California, Los Angeles, CA 90089, USA

Received 2 February 2007, Accepted 6 April 2007

The nsp14 protein is an exoribonuclease that is encoded by severe acute respiratory syndrome coronavirus (SARS-CoV). We have cloned and expressed the nsp14 protein in *Escherichia coli*, and characterized the nature and the role(s) of the metal ions in the reaction chemistry. The purified recombinant nsp14 protein digested a 5'-labeled RNA molecule, but failed to digest the RNA substrate that is modified with fluorescein group at the 3'-hydroxyl group, suggesting a 3'-to-5' exoribonuclease activity. The exoribonuclease activity requires Mg^{2+} as a cofactor. Isothermal titration calorimetry (ITC) analysis indicated a two-metal binding mode for divalent cations by nsp14. Endogenous tryptophan fluorescence and circular dichroism (CD) spectra measurements showed that there was a structural change of nsp14 when binding with metal ions. We propose that the conformational change induced by metal ions may be a prerequisite for catalytic activity by correctly positioning the side chains of the residues located in the active site of the enzyme.

Keywords: Conformational change, Exoribonuclease, Metal ions, SARS coronavirus

Introduction

In the last outbreak of SARS, the epidemic eventually spread from China to 30 countries, with more than 8,000 confirmed cases and an overall mortality rate of about 10%. A previously unknown coronavirus, SARS coronavirus (SARS-CoV), was confirmed as the agent for this epidemic (Drosten *et al*., 2003; Fouchier *et al*., 2003; Ksiazek *et al*., 2003; Peiris *et al*., 2003). Many published sequences of SARS-CoV have provided important information on the 29.7 kb positive-strand RNA genome of SARS-CoV (Marra *et al*., 2003; Rota *et al*., 2003; Ruan *et al*., 2003). Like other coronavirus, SARS-CoV gene expression and genome replication require polyprotein synthesis and subgenomic production (Miller and Koev, 2000; Ruan *et al*., 2003; Snijder *et al*., 2003; Thiel *et al*., 2003; Hussain *et al*., 2005).

Coronavirus replication in cells is initiated by translation of the two overlapping polyproteins that are proteolytically processed to yield replication-associated proteins, including RNA-dependent RNA polymerase, RNA helicase, endoribonuclease, as well as a putative exoribonuclease (Snijder *et al*., 2003; Minskaia *et al*., 2006). The possible role of the putative exoribonuclease of SARS-CoV, nsp14, in the virus replication is reported (Minskaia *et al*., 2006). The nsp14 exoribonuclease is thought to play a critical role for proof-reading, repair, and/or recombination for maintaining the integrity of the unusually long viral RNA genome of SARS coronavirus.

SARS-CoV exoribonuclease belongs to the DEDD exoribonuclease superfamily. The proteins of this family share a common catalytic mechanism characterized by the involvement of two metal ions. In the two-metal mechanism model, the first metal ion activates a water molecule to attack the P-O3' bond, while the second metal ion helps to maintain a phosphorane intermediate. To elucidate the nature and the role(s) of metal ions in the reaction chemistry, we have utilized isothermal titration calorimetry, endogenous tryptophan fluorescence and circular dichroism (CD) spectroscopy to evaluate the interactions of metal ions with the nsp14 protein. Measurement of the isotherm, fluorescence and CD signals by titration of the protein with metal ions provides a straightforward and powerful technique for evaluating the binding of metal ions to proteins. Our data provide insights on the role of metal ions in the nsp14-mediated exoribonuclease reaction.

*To whom correspondence should be addressed.
Tel: 86-27-6875 2506; Fax: 86-27-6875 2897
E-mail: dguo@whu.edu.cn

Materials and Methods

Construction of the expression plasmid pET-nsp14. The SARS-CoV cDNA was synthesized by reverse transcription using poly d(T) primer and total RNAs extracted from infected cells by the virus isolate WHU (GenBank accession number AY394850). The nsp14 gene was PCR amplified from the SARS-CoV cDNA using the following primers: The forward primer (5'-AGCCCATGGGC **CATCATCATCATCATCAC**GGATCCGCAGAAAATGTAACT GGA-3') included an *Nco*I site (underlined), a 6 × His tag sequence (bold), and a *BamH*I site (double-underlined).The reverse primer (5'-CTGCAGTCGAC**TTA**CTGTAACCTGGTAAATGT-3') included a stop codon (TAA) (bold) and a *Sal*I site (underlined). After digestion with *Nco*I and *Sal*I, the PCR product was inserted into the *Nco*I and *Sal*I sites of the vector pET-28a. The resultant plasmid, pET-nsp14, encodes SARS-CoV nsp14 with an additional MGHHHHHHGS sequence in the N-terminus.

Protein expression and purification. Plasmid pET-nsp14 was transformed into *Escherichia coli* BL21 (DE3) cells. Cultures were grown at 37°C in 1 liter of LB medium containing kanamycin (50 μg/ml) until the A600 reached 0.8 and then the expression was induced with 0.5 mM isopropyl-1-thio--D-galactopyranoside at 20°C for 16 h. The cells were harvested by centrifugation at 5,000 × g for 10 min. The pelleted cells were suspended in buffer A (40 mM Tris-HCl, pH 8.0, 100 mM NaCl, 10 mM imidazole, 7.5 mM 2-mercaptoethanol) at 10% of the original culture volume. After cell lysis by sonication, the cell lysate was separated by centrifugation at 24,000 × g for 20 min. The filtrated supernatant was applied to a nickel-nitrilotriacetic acid column (Qiagen) equilibrated by 50 ml of buffer A. After washing with 100 ml of buffer A, the nsp14 was eluted with the gradient of 1-100% buffer B (40 mM Tris-HCl, pH 8.0, 100 mM NaCl, 250 mM imidazole, 7.5 mM 2-mercaptoethanol). The eluted protein was concentrated by ultra-filter and further purified by gel filtration with Superdex G75 (Amersham). The purified protein was confirmed by sodium dodecyl sulfate-polyacrylamide (SDS-PAGE) gel electrophoresis. The protein was quantified using BioRad protein assay kit.

Preparation of nuclease substrates. To test both single-stranded and double-stranded ribonuclease activity, we used a hairpin RNA as substrate. For this, a chemically synthesized, hairpin RNA-encoding DNA sequence (GGATCCCGCATTCTATCCTCTAGA GGATGTTCAAGAGACATCCTCTAGAGGATAGAATGTTTTT TGGAAAAGCTT) was ligated into the *BamH*I-*Hind*III site of pCR3.1 vector. The DNA construct was digested with *EcoR*I and transcribed by T7 RNA polymerase *in vitro* to generate a 141-nt-hairpin RNA. The RNA was purified and labeled at the 5'-end with T4 polynucleotide kinase and [γ-^{32}P] ATP. 3'-terminal Cy3-labeled RNA was chemically synthesized. ssDNA was synthesized and labeled at 5'-end with T4 polynucleotide kinase and [γ-^{32}P] ATP. dsDNA was prepared by heating mixtures of a 5'-^{32}P-labeled oligonucleotide and its complementary oligonucleotide (molar rations, ~1 : 1.2) to 100°C for 5 min followed by slow cooling to room temperature to anneal the two strands in a Tris-HCl buffer (pH7.0) containing 100 mM of NaCl.

Exonuclease assays. The standard RNA nuclease assay was carried out as previously described (Astrom, Astrom, and Virtanen, 1992; Caruccio and Ross, 1994; delCardayre and Raines, 1994; Chekanova *et al.*, 2002). Briefly, standard reaction volume including 1 kBq (27 nCi) of radiolabeled RNA substrate and 2.3 μM of nsp14 in a buffer consisting of 50 mM Tris-HCl (pH 8.0), 50 mM KAc, 2 mM dithiothreitol, 10% glycerol, 0.1 mg/ml BSA, 5 mM $MgAc_2$, 25 mM NaH_2PO_4. The reaction mixture was incubated at 37°C for 2 min unless stated otherwise. Reactions were terminated by the addition of the equal volumes of gel-loading buffer (containing 96% formamide and 1 mM EDTA). The mixture was heated to 85°C for 2 min and put to ice bath immediately. Products were analyzed by denaturing gels composed of 7 M urea and 8% polyacrylamide. Gels were dried and exposed to a PhosphorImager screen (Amersham Biosciences). The gel using a Cy3-labeled RNA substrate was scanned directly. Quantification of radiolabeled bands was performed using ImageQuant software (Amersham Biosciences).

CD spectroscopy. The circular dichroism (CD) spectra were recorded using a Jasco J-810 spectropolarimeter at 20°C. A cell with a path length of 1 mm was used. Each spectrum was the average of four scans corrected by subtracting a spectrum of the buffer solution in the absence of protein recorded under identical condition. Each scan in the range of 200-250 nm for far-UV CD and of 250-350 nm for near-UV CD spectra was obtained by taking data points every 0.5 nm with integration time of 1s and a 2 nm bandwidth.

Fluorescence measurements. All fluorescence measurements were performed in a RF-5301PC spectrofluorophotometer. Slit widths with a nominal band pass of 3 nm were used for both excitation and emission beams. Intrinsic fluorescence emission spectra were recorded from 300 to 500 nm after exciting at 275 nm.

Isothermal titration calorimetry. ITC experiments were performed using a MicroCal VP-ITC microcalorimeter. Samples of nsp14 were dialyzed overnight at 4°C against chelex-100 treated ITC buffer containing 20 mM HEPES pH 8.0, 50 mM KCl. Protein concentration was determined using BioRad protein assay kit. Metal salts were made up in the same ITC buffer to the desired concentration. All experiments were performed at 25°C. In brief, 100-300 μM protein solution was loaded into the calorimeter cell and the injection syringe was then loaded with divalent metal ion solution. After initial 2 min delay, 28 serial of 10 μl metal ion solution were injected into the cell from the syringe using a 300 r.p.m stirring speed. An injection delay of 360 s was utilized to allow for the baseline to return after each injection. Separate experiments were conducted to measure the change of heat. A titration into ITC buffer was subtracted from the data to correct for background heat effects of dilution. Data were fit to appropriate binding models and thermodynamic parameters determined from nonlinear least-square fits by using the ORIGIN software.

Results and Discussion

The ribonuclease activity of SARS-CoV protein nsp14. The SARS-CoV nsp14 was expressed in *E. coli* with a 6 × His tag fused at the N-terminus. The fusion protein was purified

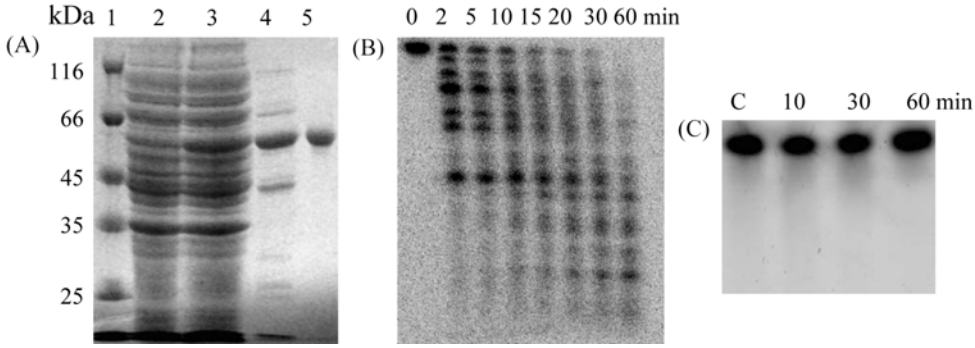

Fig. 1. The exoribonuclease activity of recombinant SARS-CoV nsp14. (A) SDS-PAGE of the nsp14 protein purified from *E. coli* cells. Lane 1: molecular weight makers, lane 2: uninduced cell lysate, lane 3: induced cell lysate, Lane 4: protein eluted from NTA-Ni^{2+} affinity column, Lane 5: the nsp14 purified by gel filtration chromatography on Superdex-75 column. (B) The exoribonuclease activity associated with the purified nsp14. (C) Inhibition of exonuclease activity by 3'-modification of the RNA substrate.

by Ni-NTA affinity column (Fig. 1A lane 4). By an additional step of gel filtration chromatography on Superdex-75 column (Amersham, Inc) the protein was purified to near homogeneity (Fig. 1A, lane 5).

To determine whether nsp14 has the ribonuclease activity, the protein was incubated with a 141-nucleotide (nt)-long hairpin RNA that was radiolabeled at the 5' end. As shown in Fig. 1b, nsp14 readily hydrolyzed 5'-labeled RNA to a set of RNAs of smaller sizes, which showed a laddering pattern of hydrolytic products, indicating that the nsp14 may possess a 3' to 5' exoribonuclease activity. The uneven distribution of the hydrolytic RNA bands suggested that the exonuclease activity may have preference for specific 3'-nucleotides and/or structures. It could also be observed that the longer the incubation period, the more extensive the hydrolytic reaction (Fig. 1B). To confirm that the nsp14 exonuclease acted in 3' to 5' polarity, we synthesized 21-nt ssRNA and labeled its 3'-hydoxy group with Cy3 fluorescein, and the nuclease assay showed that the 3'-labeling with Cy3 blocked the nucleolytic activity of nsp14 (Fig. 1C), thus suggesting that nsp14 exonuclease acted in the 3' to 5' direction. In contrast, the activity of 5' to 3' exonuclease and endonuclease do not have any requirement for 3'-structure. When the 5'-labeled ssDNA and dsDNA was incubated with nsp14, nucleolytic activity could not be observed after over one hour incubation period (data not shown). Taken together, it can be concluded that SARS-CoV nsp14 possesses a 3' to 5' exoribonuclease activity.

Effect of divalent cations on nsp14 activity. The concentrations and types of divalent cations influence the specificity and efficiency of various exonuclease reactions (Plchova, Hartung, and Puchta, 2003). For that reason, we examined the effects of three different divalent cations (Mg^{2+}, Mn^{2+} and Zn^{2+}), on the nsp14 exoribonuclease activity on the same 141 nt RNA substrate (Fig. 2A). The result showed that the nsp14 has the highest exoribonuclease activity in the presence of Mg^{2+} at even the lowest concentration tested (0.5 mM, Fig. 2A, lane 2). However, the exoribonuclease activity of nsp14 is greatly reduced in the presence of Mn^{2+} (Fig. 2A, lanes 7-11). The activity is even less in the presence of Zn^{2+}, with near background activity (Fig. 2A, lanes 12-16). The enzymatic activities at different cation conditions were quantified by counting the uncleaved full-length substrate RNA (Fig. 2B). There was less uncleaved substrate RNA left in presence of Mg^{2+} than Mn^{2+} and Zn^{2+} (Fig. 2B), suggesting the requirement for Mg^{2+} for optimal enzymatic activity. Therefore, we speculate that the exoribonuclease activity needs Mg^{2+} as a cofactor. As previous studies showed, magnesium may play structural and catalytic roles in many cellular processes that affect genome stability (Hartwig, 2001). Mg^{2+} functions as a cofactor of proteins involved in DNA replication and repair pathways. It is required for activity and fidelity of DNA polymerases (Sirover and Loeb, 1977). It is also required for the activities of nucleases, such as for AP endonuclease (Barzilay *et al*., 1995) and MutH (Welsh *et al*., 1987) nucleases, which are involved in many DNA repair pathways, including nucleotide excision repair (NER), base excision repair (BER), and DNA mismatch repair (MMR).

Thermodynamic characterization of metal ion binding to nsp14 protein. To gain an energetic and mechanistic understanding of the metal ion binding to nsp14 protein, we used ITC experiment to directly characterize the thermodynamics of the divalent metal ions binding to nsp14 (Fig. 3). As the binding of divalent metal cations to nsp14 was generally found to be endothermic, the upward peaks indicate heat uptake on injection of divalent cation solution into the nsp14 protein solution. The isotherm of titration of Mg^{2+}, Mn^{2+} or Zn^{2+} into nsp14 were fit to a two-site binding model (Microcal Origen ITC software), meaning that nsp14 has two metal ion binding sites. From sequence comparison, nsp14 belongs to DEDD exoribonuclease superfamily, and the proteins of this family share a common catalytic mechanism characterized by the involvement of two metal ions. In the two-metal mechanism model, one metal ion is involved both in positioning the substrate and in the activation of an incoming nucleophile

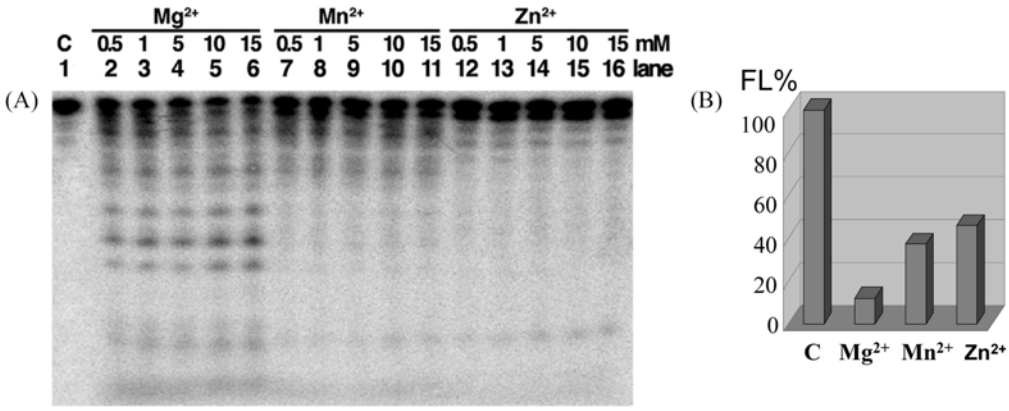

Fig. 2. Characterization of ion dependence of the exoribonuclease activity of SARS-CoV nsp14. (A). Effect of different divalent cations on the exoribonuclease activity. The exonuclease activity assay was carried out using the same buffer condition as in Fig. 1B, excepting that no $MgAc_2$ (or any other divalent cations) was present. Various concentrations of Mg^{2+} ($MgAc_2$), Mn^{2+} or Zn^{2+}, as indicated above the gel, were added to the reaction mixtures. Lane 1 is RNA substrate only. (B). The quantification of the exoribonuclease activity. Uncleaved full-length substrate RNA was quantified and shown as a percentage of input full-length RNA ([FL (%)]), thus the lower the FL percentage, the higher the exoribonuclease activity. The lanes 2, 7 and 12 for Mg^{2+}, Mn^{2+} and Zn^{2+}, respectively, in Fig. 2A were measured. The "C" (control) refers to the RNA incubation without adding nsp14 protein (lane 1 in Fig. 2A).

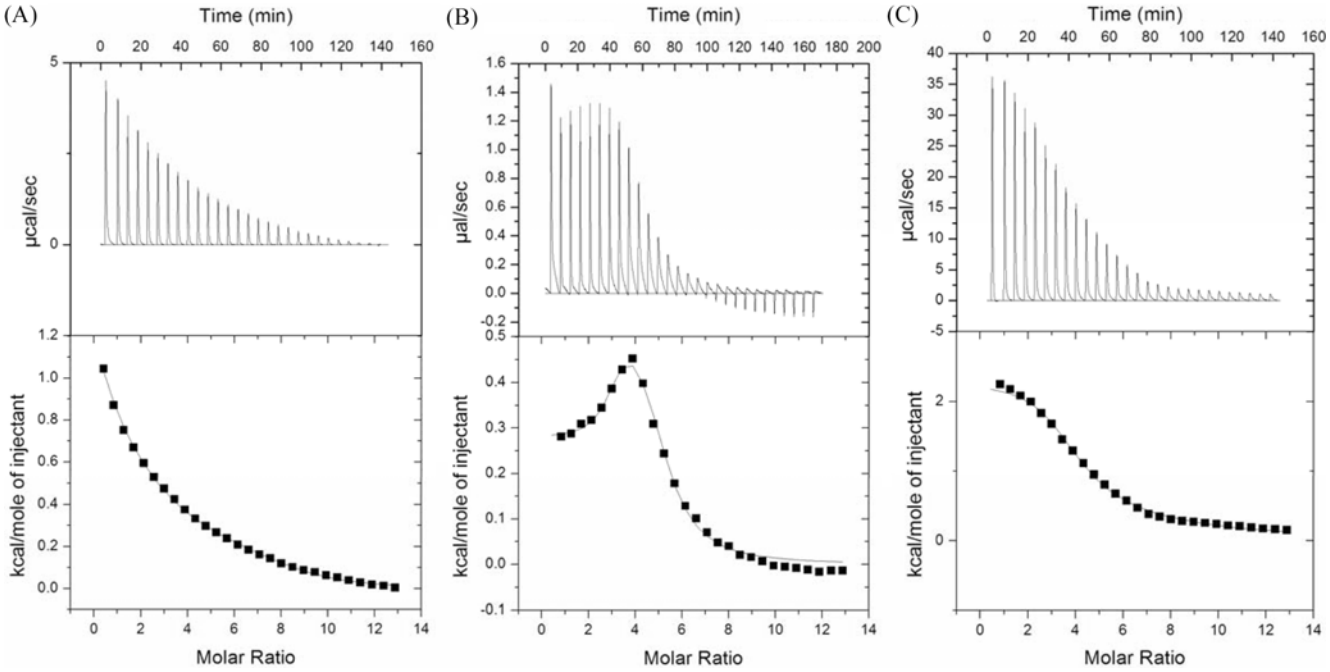

Fig. 3. Isothermal calorimetry (ITC) characterization of divalent cation binding modes by nsp14. (A, B, and C). Isothermal calorimetry (ITC) characterization of binding mode of nsp14 by Mg^{2+} (panel A), Mn^{2+} (panel B), and Zn^{2+} (panel C). Data were fit to appropriate binding models and thermodynamic parameters determined from nonlinear least-square fits, using the ORIGIN software.

(Beese and Steitz, 1991). Nucleophilic attack then generates a trigonal bipyramidal transition state that is stabilized by both metal ions. The second metal ion also stabilizes the negative charge that appears on the leaving 3' oxygen, thus facilitating its departure from the phosphate. Our results provide a thermodynamic basis of the divalent metal ions binding to nsp14. However, it is unclear whether there was a structural change during the binding process that leads to the different activity effect on the protein. To elucidate the nature and the role(s) of metal ions in the reaction chemistry, we further utilized endogenous tryptophan fluorescence and circular dichroism (CD) spectroscopy to evaluate the interactions of metal ions with the nsp14 protein.

Spectroscopic characterization of divalent ion binding to nsp14 protein. The presence of multiple tryptophan residues

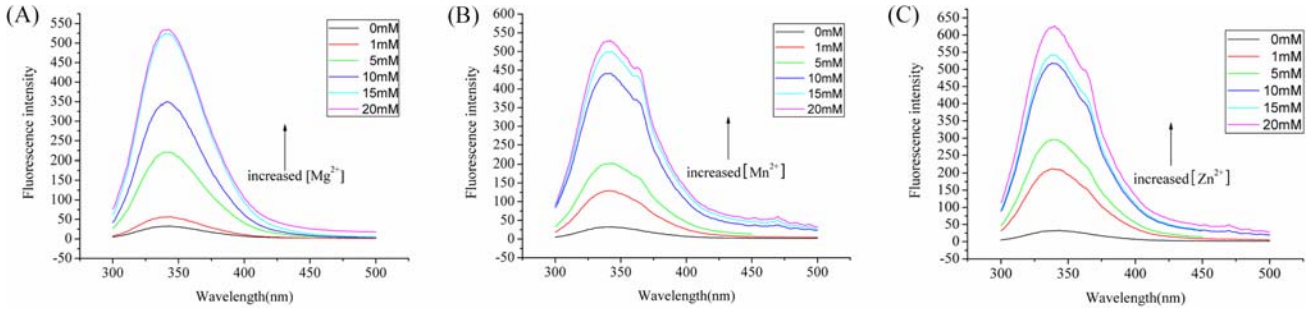

Fig. 4. Spectrofluorometric titration of nsp14 with divalent ions excitated at 275 nm. The concentration of metal ions is 0, 1, 5, 10, 15, and 20 mM. (A) Mg^{2+}, (B) Mn^{2+}, (C) Zn^{2+}.

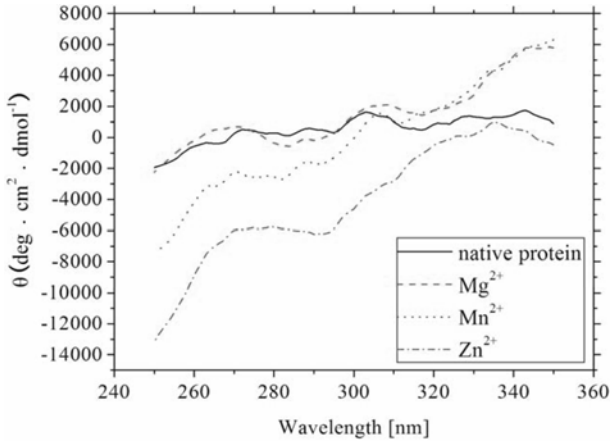

Fig. 5. Near-UV CD spectrum comparison of the nsp14 binding with divalent cations.

in the nsp14 protein allowed binding assays to be performed with a high degree of sensitivity. The fluorescence emission spectrums of nsp14 with and without divalent cations are shown in Fig. 4. The emission spectrum was a single, broad asymmetric peak centered at 343 nm; addition of metal ions did not shift the center of the peak but caused a marked enhancement of fluorescence intensity. The cations-induced fluorescence enhancements are most likely due to a conformational change in the enzyme that results in alterations in the microenvironments of tryptophan residues near the ion binding site. At the same time, we could observe the appearance of the peak at 360 nm at different concentrations of Mn^{2+} and Zn^{2+} (Fig. 4B and 4C). This new peak is very near the emission maximum of free L-tryptophan, which suggested increased exposure of Trp residues to solvent environment, resulting from the process of protein denaturation.

Interpretation of the fluorescence data in terms of spatial relationships is complicated because the tryptophan residues are distributed rather uniformly throughout the protein. To further characterize the interaction between the metal ions and nsp14, far- and near-UV CD spectra were recorded both in the presence and the absence of metal ions. Analysis of the near-UV CD spectra of the nsp14 protein in both the absence and presence of metal ions was performed from 250 to 350 nm. As can be seen in Fig. 5, native protein showed a major peak at 300 nm and two minima peak at 260 and 270 nm. After incubated with Mn^{2+} and Zn^{2+}, the protein showed a significant reduction of the CD intensity over the 260-300 nm region and the disappearance of the peak at 300 nm when the protein incubated with Zn^{2+}. Near-UV CD was used to monitor the side chain tertiary structures of proteins. The peak at 300 nm mainly reflects the structure of Trp. The decreased near-UV CD signal and the disappearance of the peak at 300 nm may reflect the loosening of protein structure by partial unfolding. On the other hand, the spectrum showed minor intensity change except the appearance of a broad asymmetric peak centered at 268 nm and a minor red shift of the 300 nm peak when the protein incubated with Mg^{2+}. This implied a structural rearrangement of nsp14 incubated with Mg^{2+}, which is further emphasized by the increase in tyrptophan fluorescence intensity.

The effects of the three divalent cations on the nsp14 protein measured by the far-UV CD spectra analysis were shown in Fig. 6 and the result indicated that the α-helicity of nsp14 was changed in the presence of Mg^{2+}, Mn^{2+} and Zn^{2+}, implying that the nsp14 protein needs low concentration divalent cations to change its conformation to stimulate the RNA hydrolysis. In fact, structural change is essential to proceed in the enzyme catalytic cycle (Hammes-Schiffer, 2002). For deoxyribonuclease, to allow DNA cutting, strand passing and rejoining, the protein must produce the conformational changes to open and close the protein gate (Sissi *et al*., 2005). Comparably, the α-helicity of nsp14 dramatically reduced when the protein incubated with high concentration of Mn^{2+} and Zn^{2+}, which imply radical conformal change. This is in agreement with the fluorescence spectrum. Thus we speculate that there is some dependability between the conformational changes with the effect of metal ion on the nsp14 nuclease activity.

Coronaviruses contain an extraordinarily large RNA genome and the large RNA size imposes a severe burden on the virus because such RNA can be expected to accumulate a large number of errors during RNA replication, assuming that error

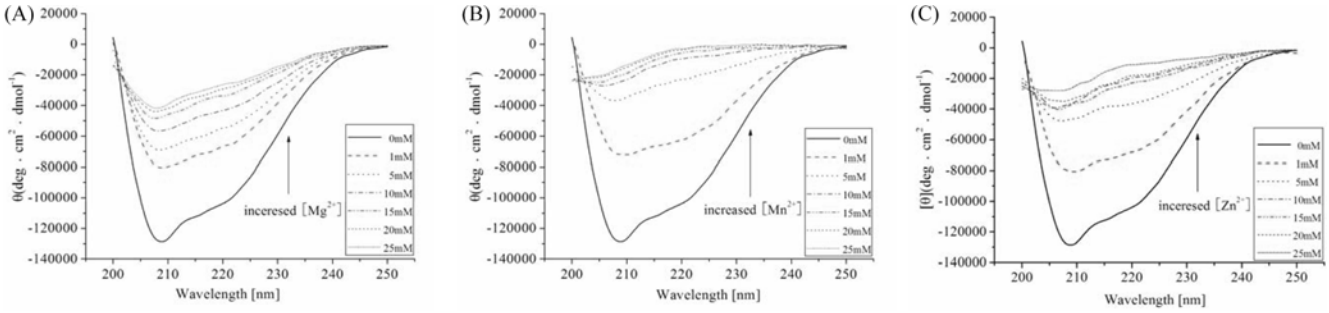

Fig. 6. Far-UV CD spectra of nsp14 in the presence of divalent cations: Mg^{2+} (A), Mn^{2+} (B), Zn^{2+} (C).

frequency of coronaviral RNA polymerase is comparable to that of other RNA viruses. Thus, coronaviruses must develop genetic mechanisms to counter the potentially deleterious effects of the errors (Lai, 1996). On the basis of its sequence similarity with cellular 3'-to-5' exonuclease, SARS-CoV nsp14 was assumed to be involved in proofreading, repair, and/or recombination (Snijder *et al*., 2003). Although the understanding of the mechanisms underlying these processes is still incomplete, characterization of the biochemical properties of nsp14 should provide the basis for further studies in this direction.

Based on the results of our fluorescence and CD experiments, we demonstrated that nsp14 undergoes conformational changes upon the binding of metal ions. This is in agreement with many other polymerases, in which major domain rearrangements are needed to form a catalytically active site (Doublie *et al*., 1998; Huang *et al*., 1998). We thus envisage that the ion-induced conformational change is a prerequisite for catalytic activity by correctly positioning the side chains of residues located in the active site of the enzyme, while at the same time contributing to the stabilization of the intermediate transition state. A number of acidic amino acid residues located in the active site of the nsp14 protein have the potential to coordinate metal ions through a network of hydrogen bonds. Following the binding of metal ions, the original hydrogen bonding interactions would be replaced by interactions with metal ions and possibly with water molecules, positioning the residues for efficient enzymatic catalysis. Further analysis by site-directed mutagenesis will precisely identify the role of these residues and provide additional information on the enzymatic activity and its catalytic mechanism.

Acknowledgments We thank Mu Xiao, Zhiqiang Chen and Peng Zhang for their help and Dr Yi Liang for advice in some of the experiments. This study was supported by China National Science Foundation (#30570394), National Basic Research Program of China (#2006CB504300) and the MOE "111" project #B06018. Guo's lab is supported by the Luojia Professorship Program of Wuhan University.

References

Astrom, J., Astrom, A. and Virtanen, A. (1992) Properties of a HeLa cell 3' exonuclease specific for degrading poly(A) tails of mammalian mRNA. *J. Biol. Chem.* **267**, 18154-18159.

Barzilay, G., Mol, C. D., Robson, C. N., Walker, L. J., Cunningham, R. P., Tainer, J. A. and Hickson, I. D. (1995) Identification of critical active-site residues in the multifunctional human DNA repair enzyme HAP1. *Nat. Struct. Biol.* **2**, 561-568.

Beese, L. S. and Steitz, T. A. (1991) Structural basis for the 3'-5' exonuclease activity of Escherichia coli DNA polymerase I: a two metal ion mechanism. *Embo J.* **10**, 25-33.

Caruccio, N. and Ross, J. (1994) Purification of a human polyribosome-associated 3' to 5' exoribonuclease. *J. Biol. Chem.* **269**, 31814-31821.

Chekanova, J. A., Dutko, J. A., Mian, I. S. and Belostotsky, D. A. (2002) Arabidopsis thaliana exosome subunit AtRrp4p is a hydrolytic 3'-->5' exonuclease containing S1 and KH RNA-binding domains. *Nucleic Acids Res.* **30**, 695-700.

delCardayre, S. B. and Raines, R. T. (1994) Structural determinants of enzymatic processivity. *Biochemistry* **33**, 6031-6037.

Doublie, S., Tabor, S., Long, A. M., Richardson, C. C. and Ellenberger, T. (1998) Crystal structure of a bacteriophage T7 DNA replication complex at 2.2 A resolution. *Nature* **391**, 251-258.

Drosten, C., Gunther, S., Preiser, W., van der Werf, S., Brodt, H. R., Becker, S., Rabenau, H., Panning, M., Kolesnikova, L., Fouchier, R. A., Berger, A., Burguiere, A. M., Cinatl, J., Eickmann, M., Escriou, N., Grywna, K., Kramme, S., Manuguerra, J. C., Muller, S., Rickerts, V., Sturmer, M., Vieth, S., Klenk, H. D., Osterhaus, A. D., Schmitz, H. and Doerr, H. W. (2003) Identification of a novel coronavirus in patients with severe acute respiratory syndrome. *N. Engl. J. Med.* **348**, 1967-1976.

Fouchier, R. A., Kuiken, T., Schutten, M., van Amerongen, G., van Doornum, G. J., van den Hoogen, B. G., Peiris, M., Lim, W., Stohr, K. and Osterhaus, A. D. (2003) Aetiology: Koch's postulates fulfilled for SARS virus. *Nature* **423**, 240.

Hammes-Schiffer, S. (2002) Impact of enzyme motion on activity. *Biochemistry* **41**, 13335-13343.

Hartwig, A. (2001) Role of magnesium in genomic stability. *Mutat. Res.* **475**, 113-121.

Huang, H., Chopra, R., Verdine, G. L. and Harrison, S. C. (1998). Structure of a covalently trapped catalytic complex of HIV-1 reverse transcriptase: implications for drug resistance. *Science* **282**, 1669-1675.

Hussain, S., Pan, J., Chen, Y., Yang, Y., Xu, J., Peng, Y., Wu, Y.,

Li, Z., Zhu, Y., Tien, P. and Guo, D. (2005) Identification of novel subgenomic RNAs and noncanonical transcription initiation signals of severe acute respiratory syndrome coronavirus. *J. Virol.* **79**, 5288-5295.

Ksiazek, T. G., Erdman, D., Goldsmith, C. S., Zaki, S. R., Peret, T., Emery, S., Tong, S., Urbani, C., Comer, J. A., Lim, W., Rollin, P. E., Dowell, S. F., Ling, A. E., Humphrey, C. D., Shieh, W. J., Guarner, J., Paddock, C. D., Rota, P., Fields, B., DeRisi, J., Yang, J. Y., Cox, N., Hughes, J. M., LeDuc, J. W., Bellini, W. J. and Anderson, L. J. (2003) A novel coronavirus associated with severe acute respiratory syndrome. *N. Engl. J. Med.* **348**, 1953-1966.

Lai, M. M. C. (1996) Recombination in large RNA viruses: coronaviruses. Semin. *Virol.* **7**, 381-388.

Marra, M. A., Jones, S. J., Astell, C. R., Holt, R. A., Brooks-Wilson, A., Butterfield, Y. S., Khattra, J., Asano, J. K., Barber, S. A., Chan, S. Y., Cloutier, A., Coughlin, S. M., Freeman, D., Girn, N., Griffith, O. L., Leach, S. R., Mayo, M., McDonald, H., Montgomery, S. B., Pandoh, P. K., Petrescu, A. S., Robertson, A. G., Schein, J. E., Siddiqui, A., Smailus, D. E., Stott, J. M., Yang, G. S., Plummer, F., Andonov, A., Artsob, H., Bastien, N., Bernard, K., Booth, T. F., Bowness, D., Czub, M., Drebot, M., Fernando, L., Flick, R., Garbutt, M., Gray, M., Grolla, A., Jones, S., Feldmann, H., Meyers, A., Kabani, A., Li, Y., Normand, S., Stroher, U., Tipples, G. A., Tyler, S., Vogrig, R., Ward, D., Watson, B., Brunham, R. C., Krajden, M., Petric, M., Skowronski, D. M., Upton, C. and Roper, R. L. (2003) The Genome sequence of the SARS-associated coronavirus. *Science* **300**, 1399-1404.

Miller, W. A. and Koev, G. (2000) Synthesis of subgenomic RNAs by positive-strand RNA viruses. *Virology* **273**, 1-8.

Minskaia, E., Hertzig, T., Gorbalenya, A. E., Campanacci, V., Cambillau, C., Canard, B. and Ziebuhr, J. (2006) Discovery of an RNA virus 3'->5' exoribonuclease that is critically involved in coronavirus RNA synthesis. *Proc. Natl. Acad. Sci. USA* **103**, 5108-5113.

Peiris, J. S., Lai, S. T., Poon, L. L., Guan, Y., Yam, L. Y., Lim, W., Nicholls, J., Yee, W. K., Yan, W. W., Cheung, M. T., Cheng, V. C., Chan, K. H., Tsang, D. N., Yung, R. W., Ng, T. K. and Yuen, K. Y. (2003) Coronavirus as a possible cause of severe acute respiratory syndrome. *Lancet* **361**, 1319-1325.

Plchova, H., Hartung, F. and Puchta, H. (2003) Biochemical characterization of an exonuclease from Arabidopsis thaliana reveals similarities to the DNA exonuclease of the human Werner syndrome protein. *J. Biol. Chem.* **278**, 44128-44138.

Rota, P. A., Oberste, M. S., Monroe, S. S., Nix, W. A., Campagnoli, R., Icenogle, J. P., Penaranda, S., Bankamp, B., Maher, K., Chen, M. H., Tong, S., Tamin, A., Lowe, L., Frace, M., DeRisi, J. L., Chen, Q., Wang, D., Erdman, D. D., Peret, T. C., Burns, C., Ksiazek, T. G., Rollin, P. E., Sanchez, A., Liffick, S., Holloway, B., Limor, J., McCaustland, K., Olsen-Rasmussen, M., Fouchier, R., Gunther, S., Osterhaus, A. D., Drosten, C., Pallansch, M. A., Anderson, L. J. and Bellini, W. J. (2003) Characterization of a novel coronavirus associated with severe acute respiratory syndrome. *Science* **300**, 1394-1399.

Ruan, Y. J., Wei, C. L., Ee, A. L., Vega, V. B., Thoreau, H., Su, S. T., Chia, J. M., Ng, P., Chiu, K. P., Lim, L., Zhang, T., Peng, C. K., Lin, E. O., Lee, N. M., Yee, S. L., Ng, L. F., Chee, R. E., Stanton, L. W., Long, P. M. and Liu, E. T. (2003) Comparative full-length genome sequence analysis of 14 SARS coronavirus isolates and common mutations associated with putative origins of infection. *Lancet* **361**, 1779-1785.

Sirover, M. A. and Loeb, L. A. (1977) On the fidelity of DNA replication. Effect of metal activators during synthesis with avian myeloblastosis virus DNA polymerase. *J. Biol. Chem.* **252**, 3605-3610.

Sissi, C., Marangon, E., Chemello, A., Noble, C. G., Maxwell, A. and Palumbo, M. (2005) The effects of metal ions on the structure and stability of the DNA gyrase B protein. *J. Mol. Biol.* **353**, 1152-1160.

Snijder, E. J., Bredenbeek, P. J., Dobbe, J. C., Thiel, V., Ziebuhr, J., Poon, L. L., Guan, Y., Rozanov, M., Spaan, W. J. and Gorbalenya, A. E. (2003) Unique and conserved features of genome and proteome of SARS-coronavirus, an early split-off from the coronavirus group 2 lineage. *J. Mol. Biol.* **331**, 991-1004.

Thiel, V., Ivanov, K. A., Putics, A., Hertzig, T., Schelle, B., Bayer, S., Weissbrich, B., Snijder, E. J., Rabenau, H., Doerr, H. W., Gorbalenya, A. E. and Ziebuhr, J. (2003) Mechanisms and enzymes involved in SARS coronavirus genome expression. *J. Gen. Virol.* **84**, 2305-2315.

Welsh, K. M., Lu, A. L., Clark, S. and Modrich, P. (1987). Isolation and characterization of the Escherichia coli mutH gene product. *J. Biol. Chem.* **262**, 15624-15629.

Ziebuhr, J. (2005) The Coronavirus Replicase; in *Coronavirus Replication and Reverse Genetics*, Enjuanes, L. (ed.), pp. 58-94, Springer, Berlin, Germany.